NASA Technical Memorandum 82796

The Dryout Region in Frictionally Heated Sliding Contacts

R. C. Hendricks
Lewis Research Center
Cleveland, Ohio

and

J. Braun
University of Akron
Akron, Ohio

and

V. Arp and P. J. Giarratano
NBS-Boulder
Boulder, Colorado

Prepared for the
Seventh International Heat Transfer Conference
sponsored by the American Society of Mechanical Engineers
Munich, Federal Republic of Germany, September 6–10, 1982

NASA

THE DRYOUT REGION IN FRICTIONALLY HEATED SLIDING CONTACTS

R. C. Hendricks, J. Braun*, V. Arp**, and P. J. Giarratano**

National Aeronautics and Space Administration
Lewis Research Center
Cleveland, Ohio 44135

ABSTRACT†

Some conditions under which boiling and two-phase flow can occur in or near a wet sliding contact are determined and illustrated. The experimental apparatus consisted of a tool pressed against an instrumented slider plate and motion picture sequences at 400 frames/sec. The temperature and photographic data demonstrated surface conditions of boiling, drying, trapped gas evolution (solutions), and volatility of fluid mixture components. The theoretical modeling and analysis are in reasonable agreement with experimental data.

INTRODUCTION†

When two dry surfaces are in sliding contact, frictional heating occurs near the interface in the zone of true contact giving rise to severe temperature gradients directly related to sliding velocity, surface roughness, and applied load.

E-1130

Heat transfer in sliding contacts, bearings, and seals possesses a commonality - very thin films. In some cases, the films may be of the 'dry' or third body types as discussed in a universal appraoch to tribology by Godet et al. [1]. Others may be classified as 'wet' and many applications and theories of wet-contacts, including the third body approach [1], exist in the literature. Dowson et al. [2] edited the 1979 Leeds-Lyon symposium on heat transfer in bearings and other forms of asperity contacts such as surface roughness. Burton [3] edited a symposium on heat transfer in sliding contacts with thermoelastic behavior and more recently, Dow [4] convened a second symposium on heat transfer in dry and wet sliding contact systems including thermoelastic behavior. Marscher [5] has investigated and characterized the flash temperature usually associated with very high speed short duration rubbing contact such as a compressor or turbine blade tip against a shroud seal, which is also discussed by Bill [6]. Townsend and Akin [7] have investigated the nature of heat transfer for the complex sliding contacts associated with gear teeth. Majumdar and Hamrock [8] describe some heat transfer characteristics of rolling contacts with slip.

While these researchers have investigated the nature of heat transfer in sliding contacts, they have not investigated heat transfer and phase change in thin films. Such conditions may be responsible for the sudden

*University of Akron, Akron, Ohio 44325.
**NBS-Boulder, Boulder, Colorado 80302.
†An abridged version of this document appears as paper 82-ihtc-140 prepared for presentation at the 7th International Heat Transfer Conference, Sept. 6-10, 1982, Munich FRG.

increase in seal flow rate with subsequent 'puffing' instabilities, for the loss of lubricant film (load carrying capacity) and for the stick-slip instability, as the surface becomes alternately 'wet' and 'dry' with asperity contact. Two-phase flows in seal systems have been characterized by Hughes and Chao [9] and Lebeck [10]. Viscous two-phase flow without asperity contact was addressed in [9] and the probability of asperity contacts with a phase change interface rather than two-phase viscous flow was considered in [10].

In this paper, we will use the work of Patir and Cheng [11] to characterize film thickness and determine and illustrate some conditions under which boiling can occur in or near a wet sliding contact using a fixed tool-like surface pressed against a moving work piece.

APPARATUS AND INSTRUMENTATION

A schematic illustrating the principal components of the apparatus is given as Fig. 1. Photographs showing an overview of the apparatus are given as Fig. 2. Both the fixed wedge-shaped tool with a machined flat (0.518x10.2 mm), Fig. 1, and sliding surfaces were made of high carbon steel (C1095) commonly designated as tool steel or drill rod. The test (i.e., sliding) surface was split into two lengths with 16 vertical (0.16x0.34 mm) slots spaced at 1.6 mm milled into one surface. Eight slots ran from the keyway to the surface, while eight others ran from the keyway to subsurface positions starting at 0.03 mm depth and increasing in increments of 0.03 mm for each subsurface slot. Sixteen Chromel-Alumel thermocouples with glass insulated 0.13 mm diameter wire were fabricated; surface junctions were peened into the slots, and subsurface junctions were epoxied into position in each premachined slot. The two split lengths sandwiched and 'swagged' the thermocouples into position forming a near-continuous instrumented test configuration. The surface was then ground to assure flatness. The thermocouple leads were potted and terminated in plug connectors. The plug ends were in turn connected to a reference junction through a primary amplifier at 20:1 gain into the secondary variable gain amplifier of the high response strip chart recorder. In order to minimize pickup problems from the machine drive motors, it was necessary to mount the assembly on a Lucite plate which in turn was attached to the machine table.

The 'tool' was mounted in a special holder and attached to the rod of a hydraulic piston. A bourdon-type pressure gage was calibrated and after removal of trapped gases served to close the upper end of the hydraulic piston. Thus any movement of the piston rod would result in a pressure rise. The hydraulic cylinder with a 38-mm bore was in turn mounted on a base plate where a guide was used to minimize torque on the piston rod and provide proper alignment of the tool on the test surface. The assembly was then mounted to the vertical slide of the numerically controlled (NC)-milling machine. Vertical positioning of the slide, table motion, and position could be accomplished accurately and reproducibly via automatic and/or manual control.

OPERATIONS

The tool was automatically positioned above the test surface; it was then lowered against the surface until the desired pressure was established by manual electro-servo adjustments of the vertical slide. The system was

tion of this transition point is quite important. At point Z, there is total surface failure and seizure occurs.

Wear Particles and Surface Damage

The types of wear particles and surface damage generated during these lubrication regimes has been reported by Reda, et al. (ref. 9). In that study, wear particles were generated in sliding steel contacts and were isolated by Ferrographic analysis (ref. 10). Basically, this technique involves pumping a quantity of used lubricant across a glass slide which sits on top of an electromagnet (fig. 3). The ferromagnetic wear particles are magnetically precipitated onto the slide and can then be observed microscopically. Surface damage can also be observed by microscopic examination.

Hydrodynamic and EHD Regimes

Since the surfaces are completely separated in these regimes, no wear or surface damage should be evident. This is the case with a featureless surface (fig. 4(a)) and only a few isolated wear particles (fig. 4(b)).

Mixed and Boundary Lubrication Regimes

These are mild wear regimes where penetration of the boundary film occurs.
This produces the surface damage as illustrated in figure 5(a). Wear parti- cles are generated in a thin surface layer that is continuously removed and reformed during the sliding process. In Ferrographic terminology the wear particles generated in these regimes are referred to as normal rubbing wear particles. These flake-like particles are released into the lubricant by an exfoliation or fatigue-like process. The rate of removal of this surface layer is less than its rate of formation. Wear occurs continuously but at a low rate.

These wear particles are arranged in strings by the magnetic field of the Ferrograph (fig. 5(b)). A scanning electron micrograph (fig. 6) (ref. 11) at a higher magnification illustrates their flake-like nature. Typically, for steel surfaces, these particles are 0.75 to 1.0 μm in thickness with a major dimension of less than 15 μm.

The transition from the EHD regime into the mixed and boundary regimes is dramatically illustrated by Ferrographic analysis (fig. 7) (ref. 12). In this figure the Ferrogram density is plotted as a function of the Λ ratio. Ferrogram density is a measure of the amount of wear particles. The Λ ratio is the ratio of the film thickness to the composite surface roughness. This data was generated by sliding steel balls of three different roughnesses against a sapphire plate. As can be seen, the amount of wear debris increases sharply at Λ values of one and below where surface interactions begin taking place. The comparable curve for the friction coefficient (f) as a function of the Λ ratio appear in figure 8 (ref. 12). Here the corresponding increase in the friction with increasing surface interactions is evident. This is analogous to the rising portion of the Stribeck-Hersey curve (fig. 1) in the mixed film regime.

$$\frac{dp}{dx} = \eta \frac{d^2u}{dz^2} \tag{2}$$

The boundary conditions, considering that the horizontal table moves with respect to the stationary wedge-shaped tool, are

$$z = h \quad u = 0; \quad z = 0 \quad u = U \tag{3}$$

where

$$h(x) = H_1 + \frac{(H_0 - H_1)(B_1 - x)}{B_1} \tag{4}$$

Solving for the pressure gradient, one obtains for the smooth surface self acting thrust bearing.

$$\frac{dp}{dx} = 6\eta U \frac{(h - \bar{h})}{h^3(x)} \tag{5}$$

where

$$\bar{h} = \frac{2\kappa(\kappa - \beta B_1)}{B_1(2\kappa - \beta B_1)} \tag{6}$$

and where

$$\kappa = H_0 B_1, \ \beta = H_0 - H_1 \tag{7}$$

To account for the resistance to flow due to the surface roughness, Patir and Cheng [11] have suggested a correction factor φ for incompressible flow.

$$\varphi = 1 - 0.9 \exp\left(-0.56 \frac{h}{\sigma_s}\right) \tag{8}$$

where the surface is assumed to have isotropic roughness, with Gaussian distributions having standard deviations σ_1 and σ_2 with $\sigma_s = \sqrt{\sigma_1^2 + \sigma_2^2}$. Thus it is obvious that with part of the free flow area restricted, for the same mass flow, pressure gradients according to the modified Eq. (5) will be more severe.

$$\frac{dp}{dx} = \frac{6\eta U(h - \bar{h})}{\varphi h^3(x)} \tag{9}$$

Using the pressure gradient of Eq. (9) the shear stress becomes

$$\tau(x,z) = \left(\frac{6\eta U}{\varphi h^3(x)}\right)(h(x) - \bar{h})(z - h(x)) - \frac{\eta U}{h(x)} \tag{10}$$

and the heat generated in the process,

$$q = -\left(\frac{\eta U^2}{h^3(x)}\right) \frac{3(h(x) - \bar{h})}{\varphi h(x)} \tag{11}$$

It is evident that with $\varphi = 1$, Eq. (11) corresponds to the full unrestricted flow case.

To evaluate the temperatures, we have considered the lubricant as a medium moving across a line source of the length of the slider. For this case, Carslaw and Jaeger [22] give:

$$\vartheta = \left(\frac{q}{2\pi\lambda}\right) \int_{-b}^{b} \exp\left[\frac{U(x - x')}{2a}\right] K_0 \left\{\frac{U[(x - x')^2 + z^2]^{1/2}}{2a}\right\} dx' \tag{12}$$

Using Eqs. (11) and (12), with $\varphi < 1$ and $z = 0$, we have obtained the curves of Fig. 3. It is evident that the slope ϑ/U becomes extremely steep at high speeds.

The evaporation equation can be written as,

$$-(T_w - T_{sat})\alpha_w + \lambda\left(\frac{\partial T}{\partial z}\right) = \rho\Delta h_v \frac{dz}{dt} \tag{13}$$

By neglecting conduction into the liquid, one could very simply estimate the velocity of advance of the evaporation front

$$\frac{dz}{dt} = \frac{-\alpha_w(T_w - T_{sat})}{\rho\Delta h_v} \tag{14}$$

The results will also be related to the classic Bloc problem [18,19] as expanded by Jaeger [20], assuming that an equal amount of energy goes to the tool and the test slide surface (twice Eq. (13)),

$$y = \frac{\pi\lambda U\vartheta}{2q} = \int_{X-B}^{X+B} e^{\zeta}[K_0(Z^2 + \zeta^2)^{1/2}]\, d\zeta \tag{15}$$

where

$$B = \frac{Ub}{2a},\quad X = \frac{Ux}{2a},\quad Z = \frac{Uz}{2a} \quad \text{and} \quad \zeta = \frac{U(x - x')}{2a}$$

This solution assumes perfect contact and must be modified to include the effects of asperity contact (imperfect contact) and the effects of a thin film. The analysis of Patir and Cheng [11] provides a stochastic method of characterizing rough sliding surfaces. The average gap thickness is defined as,

$$\bar{h}_T = \int_{-h}^{\infty} (h + \delta) f(\delta)\, d\delta \tag{16}$$

where

$$\bar{h}_T = h + \delta$$

and h represents the nominal film thickness, δ the combined roughness of the sliding surfaces, and $f(\delta)$ the probability distribution function. For a normal distribution, the fraction of the surface in contact becomes,

$$X_1 = \int_{-\infty}^{-h_1} \exp\left(\frac{-\delta^2}{2\sigma_s}\right)^2 \frac{d\delta}{\sigma_s\sqrt{2\pi}} = \frac{1}{2}\,\mathrm{erfc}\left(\frac{h}{\sigma_s\sqrt{2}}\right) \tag{17}$$

and the fraction in fluid contact becomes,

$$x_2 = \frac{1}{2}\left[1 + \mathrm{erf}\left(\frac{h}{\sigma_s\sqrt{2}}\right)\right] \tag{18}$$

Thus the combined thermal diffusivity (a) and friction coefficient (u_0) may be written,

$$\begin{aligned} a &= x_1 a_s + x_2 a_f \\ u_0 &= x_1 u_{0_s} + x_2 u_{0_f} \end{aligned} \tag{19}$$

RESULTS AND DISCUSSION

Experimental Observations

Typical temperature-time histories are given as Fig. 4. Figure 4(a) represents a 75-MPa tool loading on a trichloroethane film and as one can see, the temperature differences are not more than 3° C and nearly uniform action prevails over the entire surface. Figure 4(b) represents a 750-MPa tool loading of a trichloroethane film. Significant here is the increase in temperature as the 'tool' proceeds to the third thermocouple. In the vicinity of the fourth position, the temperature suddenly drops. This is in correspondence with the appearance of bubbles in the film immediately behind

the tool. It is also clear that the film temperature ahead of the tool increases, an effect which can be seen in the work of Dow and Kannel [17] for rolling contacts. Figure 4(c) shows a 520-MPa tool loading with surface temperature characteristics similar to those of Fig. 4(b), only here the film is solvent 'WD-40.' The major difference was the appearance of very small bubbles at the tool trailing edge similar to a hydrogen bubble generator. It is speculated that such ebullition represents the evolution of the most volatile fluid mixture component, see motion picture supplement.

Analysis of Data and Simplified Theory

An analysis of the temperature time (or distance) histories is given in Fig. 5. The basic data of Fig. 5(a) represent thermocouple number 3 of Fig. 4(b). The relation between record paper distance (W) and physical distance (x) is $W = V_p x/U$, or the slider width equals (203x0.518/41.9) 2.5 mm of record paper, where V_p is paper speed and U is the slider speed. The measured system response constant ($t_c = (W/V_p)_c = 6.5/203$) of 0.03 seconds was found by step switching a series of known voltages and frequencies through the amplifier-recorder system. Persistent investigation of seemingly minor inconsistaencies lead to establishing that the system time constant, which was necessary to eliminate 60 Hz pickup, and as discussed later also partially masked thermocouple response. Considering the thermocouple, the effective width (b_e)* is ($2\,b_e = 2b + 2d = 0.581 + 0.330 = 0.848$ mm) 2.05 mm of record paper, and so the tool passing transient is somewhat masked by slow system response; the initial slopes of data shown in Fig. 5 are more characteristic of system response than tool-slider response,** but the peak-to-peak results are accurate. Comparison of these data to the classic Bloc problem [18-20] using the system response characteristic to provide the distance normalizing constant (b_e), is informative even if only qualitative.

For steel sliding on steel in air, Bisson and Anderson [21] give a maximum friction coefficient of 0.54 and lubricated surfaces can have coefficients near 0.12. Assume the fluid film thickness equal to the standard deviation of the combined roughness ($h \doteq \sigma_s$), $\mu_0 = 0.19$, and ($a_s = 0.12$, $a_f = 0.001$), $a = 0.02\times10^{-4}$ m^2/s; see section on minimum nucleation thickness. As the thermocouples are essentially in the plane, $z = 0$, a closed form solution exists as given by Carslaw and Jaeger [22] in terms of Bessel functions K_0 and K_1. For a tool velocity of 4.2 cm/s, the tool position parameter $B = U_b/2a = 2.7$ and the calculated value, maximum value, of the temperature parameter $Y_{calc} = \pi\gamma U\delta/2aq = 5.4$.

Experimentally, the temperature difference is 12.2 K, the gage pressure is 3.45 MPa (500 psig), the piston area (11.4 cm^2), the tool area (0.0526 cm^2), and the heat generated, $Aq = \mu_0 F_z U$ or $q/U = \mu_0 P$, is assumed to flow equally into the tool and the slider. The experimental maximum value of Y becomes

*A less satisfactory definition considers leading and trailing fluid envelopes such that (b_e) is doubled.

**Our primary concern was the existance of boiling and two-phase in the vicinity of the sliding contact and lesser attention given to details of the transient which will require further investigation.

$$y_{exp} = \left(\frac{\pi\lambda U\mathcal{J}}{2aq}\right)_{exp} = \frac{\pi\lambda\mathcal{J}}{a\mu_0 P} = \frac{\pi(46)(12.2)}{[(2\times10^{-6})(0.19)(3.45\times10^{6}\times11.4/0.0526)]} = 6.2$$

The analytical model (Eq. (13), Fig. 2) predicts a surface temperature difference of 10 K, and from the simplified model Y_{calc} is 11 K.* The agreement is fortuitous because of the uncertainties in (b_e), (h/σ_s) and system response. While agreement over the interval is uncertain, trailing edge effects appear to be stronger than anticipated. A more detailed analysis and experiment is certainly in order; the above represents a first approximation to a rather complex problem.

Photographic Evidence

Examination of the time-temperature data and the motion pictures revealed dry patches (Fig. 6(a)), bubbles (Fig. 6(b)), and bubble evolution (Fig. 6(c)). The associated sketches aide the reader in viewing what is more easily seen in the 16-mm motion picture supplement. The films in Figs. 6(a) and 6(b) are trichloroethane at 450 MPa and 600 MPa loading, respectively. When the film is sufficiently thin, a 'dry' surface can appear at the tool trailing edge which can be difficult to rewet. Consequently any subsequent motion across such an interface would represent a 'dry' rub with a higher coefficient of friction and a loss of material.**

When the surface is flooded, surface tension can be sufficient to drag the fluid across the surface and the film thick enough to permit visualization of bubbles generated at the tool trailing edge (Fig. 6(b)).

When the fluid mixture contains high volatility components, or is a solution with dissolved gases, bubbles are readily generated. At a film loading of 450 MPa, and a flooded surface, bubble streets and sheets are visible in solvent (WD-40) as illustrated in Fig. 6(c).

Other interesting features included the collapse of a gas bubble which came out of solution with heavy duty oil. Such a bubble collapse destroys the film adjacent to it. Silicone oils readily trap air and upon loading leave sheets of bubbles across the surface giving the appearance of dry streaks.

A motion picture supplement (C304) is available on loan which elucidates the various effects of bubble generation, dissolved gases (solutions) and mixtures with volatile components.

SUMMARY OF RESULTS

A variety of fluids have been tested in combined wet-dry sliding contact using a fixed tool pressed against an instrumented sliding flat plate. As pressure (tool loading) is increased, the surface became either dry in certain regions and exhibit boiling in the wetted regions or boiling can

*For $(h/\sigma_s) = 0.7$, $a = 0.3$, $\mu_0 = 0.22$, $B = 1.8$, $Y_{calc} = 4.2$, $Y_{exp} = 3.6$ and $T_{calc} = 14.4°$ C, which represents better agreement with data but as discussed prior, the exact value is unknown.

**In some cases, the residue may serve as a third body lubricant to prevent catastrophic damage. The residue from pure trichloroethane is generally very small.

occur along a line at the tool trailing edge. Dissolved gases and mixtures exhibit boiling characteristics although it is possible that 'outgassing' and loss of the most volatile component may occur instead. A motion picture supplement has been prepared which illustrates these processes.

An analysis of the peak temperature of the sliding contact based on the stochastic methods of Patir and Cheng exhibit reasonable agreement with the data. Further measurements and analyses are required to define the nature of the film, its thickness, and asperity interactions. It is speculated that partial film losses can contribute to failures in seals and other sliding contacts such as in bearings and gears.

ACKNOWLEDGEMENT

The authors wish to thank the Instrumentation and Machine Shop sections at LeRC for their ideas, concepts, and continuous support throughout this project.

NON-STANDARD SYMBOL LIST

A	area
a	thermal diffusivity
B_1	slider length
b	tool half width
d	thermocouple junction width
$f(\delta)$	probability function
F_z	applied normal load
$h(x)$	x-dependent film thickness
h	nominal film thickness
Δhv	latent heat
h_T	film thickness
H_0	slider inlet height
H_1	slider exit height
K_0, K_1	modified Bessel functions
p	pressure
q	heat flux
T	temperature
u	velocity
U	velocity of slider
V_p	paper speed
x	x-direction
y	y-direction
x_1	fraction of surface contact
x_2	fraction of fluid contact
$x-x'$	displaced x-coordinate
z	z-direction

DIMENSIONLESS PARAMETERS

$B = Ub/2a$	tool position parameter
$X = Ux/2a$	coordinate parameter
$Y = \pi\lambda U\sim/aq$	temperature parameter
$Z = Uz/2a$	coordinate parameter
$\zeta = U(x-x')/2a$	coordinate transform parameter

Greek Symbols

α	heat transfer coefficient
β	slider height difference ($H_0 - H_1$)
δ_T	film thickness
δ_S	combined surface roughness
κ	slider length-height product, $H_0 B_1$
λ	thermal conductivity
ϕ	flow correction factor
ρ	density
σ_S	combined standard deviation
σ	surface tension
τ	shear stress
η	dynamic viscosity
μ_0	friction coefficient
ϑ	temperature difference

Subscripts

calc	calculated
e	effective
exp	experimental
f	fluid
s	solid
T	total
v	vapor
w	wall or surface

REFERENCES

[1] Godet, M., Play, D., and Berthe, D., An Attempt to Provide a Unified Treatment of Tribology Through Load Carrying Capacity, Transport, and Continuum Mechanics, J. Lubr. Technol., vol. 102, pp. 153-164, 1980.

[2] Dowson, D., Taylor, C. M., Godet, M. and Berthe, D., Thermal Effects in Tribology. Proceedings of the 6th Leeds-Lyon Symposium on Tribology. Mech. Engr. Pub. Ltd., London, 1980.

[3] Burton, Ralph A., ed., Thermal Deformation in Frictionally Heated Systems. Elsevier Sequoia S. A., New York, 1980.

[4] Dow, T. A.: Thermomechanical Effects Workshop. Battelle-Columbus. June 17-19, 1981, Columbus, OH.

[5] Marscher, W. D., A Critical Evaluation of the Flash Temperature Concept, American Society of Lubrication Engineers 36th Annual Meeting, Pittsburgh, PA., ASLE Preprint No. 81-AM-ID-3, Park Ridge, IL, ASLE, 1981.

[6] Bill, R. C., Ludwig, L. P., Wear of Seal Materials Used in Aircraft Propulsion Systems. Wear, vol. 59, pp. 165-189, 1980.

[7] Townsend, D. P., Akin, L. S., Analytical and Experimental Spur Gear Tooth Temperatures as Affected by Operating Variables. J. Mech. Des., vol. 103, pp. 219-226, 1981.

[8] Majumdar, B. C., Hamrock, B. J., Effect of Surface Roughness on Hydrodynamic Bearings, NASA TM-81711, Oct. 1981.

[9] Hughes, W. F., Chao, N. H., Phase Change in Liquid Face Seals. II - Isothermal and Adiabatic Bounds With Real Fluids. ASME Paper 79-LUB-4, 1979.
[10] Lebeck, A. O., A Mixed Friction Hydrostatic Face Seal Model With Phase Change, ASME Paper 79-LUB-5, 1979.
[11] Patir, N, Cheng, H. S., Application of Average Flow Model to Lubrication Between Rough Sliding Surfaces. J. Lubr. Technol., vol. 101, pp. 220-230, 1979.
[12] Sharp, R. R., The Nature of Liquid Film Evaporation During Nucleate Boiling, NASA TN D-1997, Oct. 1964.
[13] Giarratano, P. J., Frederick, N. V., Transient Pool Boiling of Liquid Helium Using a Temperature-Controlled Heater Surface, in Advances in Cryogenic Engineering, eds. K. D. Timmerhaus, H. A. Snyder, vol. 25, pp. 455-466, Plenum Press, New York, 1980.
[14] Hsu, Y. Y.: On the Size Range of Active Nucleation Cavities on Heating Surfaces. J. Heat Transfer, vol. 84C, pp. 207-216, 1962.
[15] Hsu, Yih-Yun, Graham, Robert W., Transport Processes in Boiling and Two-Phase Systems, Including Near-Critical Fluids. Hemisphere, Washington, 1976.
[16] Schrage, Robert W., A theoretical Study of the Interphase Mass Transfer. Columbia Univ. Press, New York, 1953.
[17] Dow, T. A., Kannel, J. W., Evaluation of Rolling/Sliding EHD Temperatures, in Thermal Effects in Tribology, Proceedings of the 6th Leeds-Lyon Symposium on Tribology. Mech. Eng. Pub. Ltd., London, pp. 228-240, 1980.
[18] Blok, H., Theoretical Study of Temperature Rise at Surfaces of Actual Contact Under Oiliness Lubricating Conditions, in General Discussion on Lubrication and Lubricants - Group IV: Properties and Testing, Inst. Mech. Eng., London, Proc., vol. 2, p. 222, 1937.
[19] Blok, H., Fundamental Mechanical Aspects of Boundary Lubrication, SAE J., vol. 46, pp. 54-68, 1940.
[20] Jaeger, J., "Moving Sources of Heat and Temperature at Sliding Contacts," Proc. Roy. Soc. New South Wales, vol. 76, pp. 203-224, 1943.
[21] Bisson, E. E., Anderson, W. J., Advanced Bearing Technology. NASA SP-38, 1964.
[22] Carslaw, H. S., Jaeger, J. C., Conduction of Heat in Solids. 2nd ed., Clarendon Press, Oxford, 1959.
[23] Bird, Robert Byron, Stewart, Warren E., Lightfoot, Edwin, N.: Transport Phenomena. John Wiley, New York, 1960.
[24] Rohsenow, Warren M., Hartnett, James P., Handbook of Heat Transfer. McGraw-Hill, New York, 1973.

APPENDIX - MOTION PICTURE SUPPLEMENT

When two dry surfaces are in sliding contact, frictional heating occurs near the interface in the zone contact and gives rise to severe temperature gradients directly related to sliding velocity, surface roughness, and applied load. Heat transfer in sliding contacts, bearings, and seals possesses a commonality - very thin films. In some cases, the films may be of the "dry" types. Others may be classified as "wet." Or in general, all may be thought of as third-body types as discussed in a universal approach to tribology by Godet.

Several lubricant fluids were tested in an apparatus consisting of a wedge-shaped tool surface with a machined flat pressed against an instrumented plate that was attached to the bed of a numerically controlled machine. The results are discussed and illustrated in the motion picture supplement. The bed speed was fixed at 203 mm/s and the applied load varied.

Motion picture sequences taken at 400 frames/sec of the tool trailing edge show dryout or loss of lubricant, ebullition or boiling and two-phase transitions, trapped-gas evolution, and the volatility of fluid mixture components. The lubricant fluids illustrated include water, ethanol, heavy-duty oil (synthetic), spindle oil, trichloroethane, solvent (WD-40), and silicone oil.

Overview of the Various Fluids Tested

Water. - Large surface tension effects, are illustrated in two sequences. The first shows a large water droplet pushed ahead of the tool on a surface that appears to be scraped clean. The second shows the effects of surface tension at the trailing edge of the tool. Careful observation shows some boiling (bubbles) within the film at the tool trailing edge.

Ethanol. - Ethanol beads in front of the tool. The surface is wet prior to the start of motion but appears to be scraped clean in places as small streaks appear with some small possible bubbling in the wake.

Heavy-duty oil. - A synthetic oil appears to possess good load capacity. The heavy-duty oil appears to wet the surface, with some bubbling starting at the tool right edge. Surface streaks also appear.

Spindle oil. - This oil wets the surface but has little load capacity. Bubbling occurs in the fluid wedge, and bubble streaks appear on the surface. A very peculiar surface tension effect is noted at the end of the load cycle.

Trichloroethane. - This fluid wets the surface readily and has good load capacity. A most interesting bouncing droplet appears as the tool is lifted. The droplet appears to evaporate and lose fluid simultaneously before its entrainment into the surface.

Solvent. - A solvent illustrates the effects of the release of the most volatile component. Trailing edge bubbles indicate the volatile component evolution (ebullition). Bubbles also appear from the side of the tool, indicating preheating of the fluid.

Silicone oil. - This type of oil readily traps air, and bubble streaks appear behind the tool. Dissolved gases have a significant effect on lubricants, to the point that without such gases, they may not lubricate at all.

Boiling from Tool and Drying of Surface

Trichloroethane. - The fluid film is loaded to 450 MPa (65 ksi). A dry streak appears on the surface but tends to close near the end of the sequence, indicating perhaps a maldistribution of the fluid film or significant cooling due to evaporation. Increasing the load to 600 MPa (86.8 ksi) and permitting heavy liquid film at the trailing edge results in bubbles that are easily seen through the fluid film.

Solvent. - When the solvent is located to 450 MPa (65 ksi), bubbles appear at the tool trailing edge like a hydrogen bubble generator. The most volatile component is assumed to be emerging from the tool interface.

Silicone oil. - Loading the oil to 450 MPa (65 ksi) shows dissolved gas streaks, illustrating the effects of trapped gases and possible combined ebullition and evolution.

Heavy-duty oil. - When the synthetic oil is loaded to 750 MPa (108.6 ksi), we note the collapse of a dissolved gas bubble, small bubble streaks, and some boiling, which occurs in the fluid wedge at the right side of the tool. The dryer portion of the surface is evidently hotter, but the film is too thin to generate bubbles.

Summary

The motion picture supplement illustrates that various types of phase change can and do occur in frictionally heated sliding contacts. A composite view is presented where the effects of drying, boiling, volatility of solutions, and trapped gases can be visualized. It should be clear that this study of the problems in frictionally heated sliding contacts has merely begun and much more effort will be required for an understanding of such a complex process.

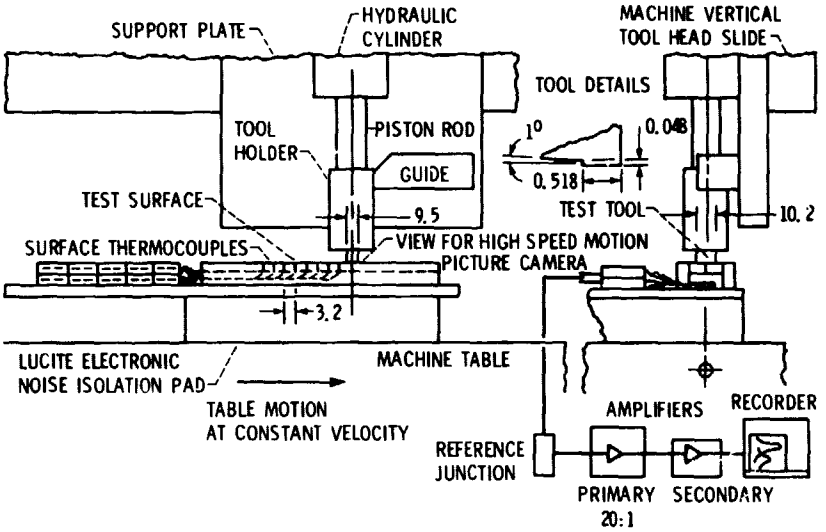

Figure 1. - Schematic of surface slider apparatus. Dimensions in millimeters.

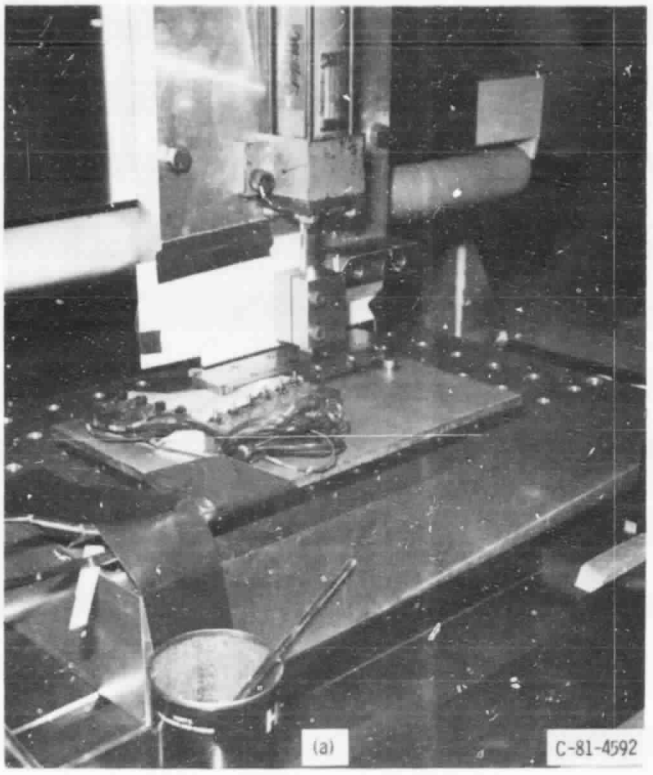

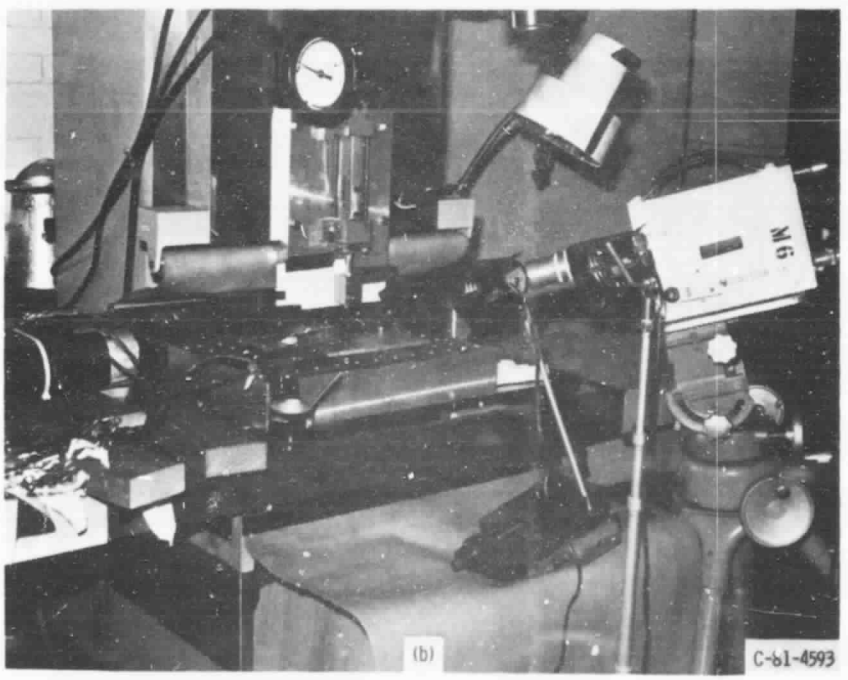

Figure 2. - Photograph of test apparatus mounted on a NC-machine.

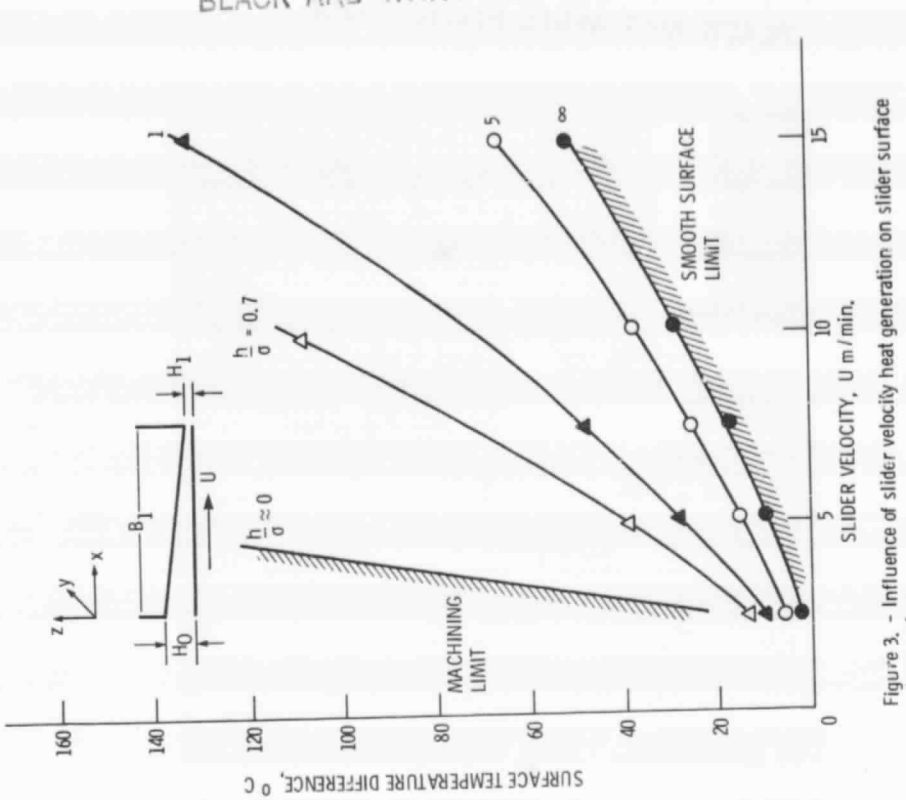

Figure 3. - Influence of slider velocity heat generation on slider surface temperature.

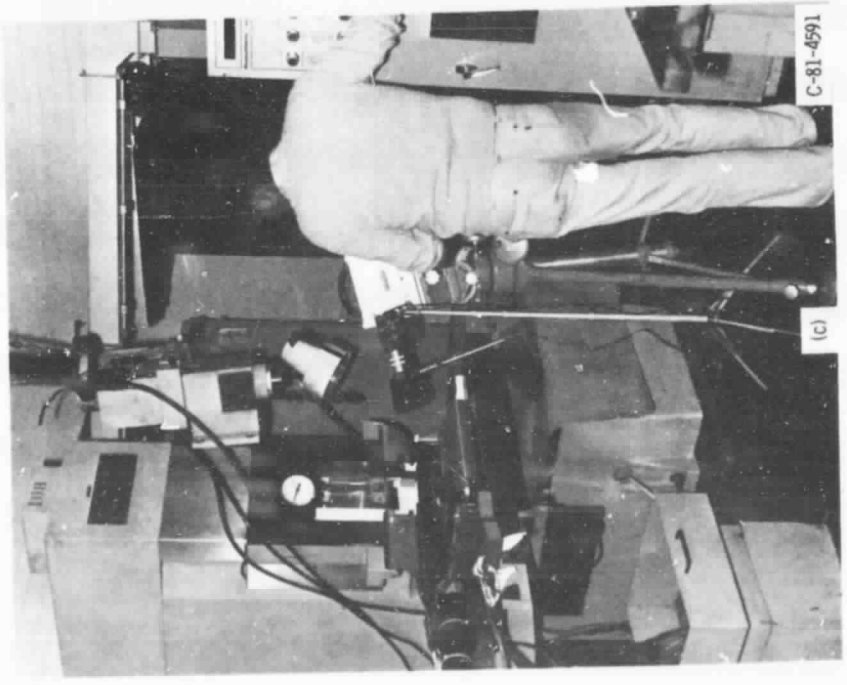

Figure 2. - Concluded.

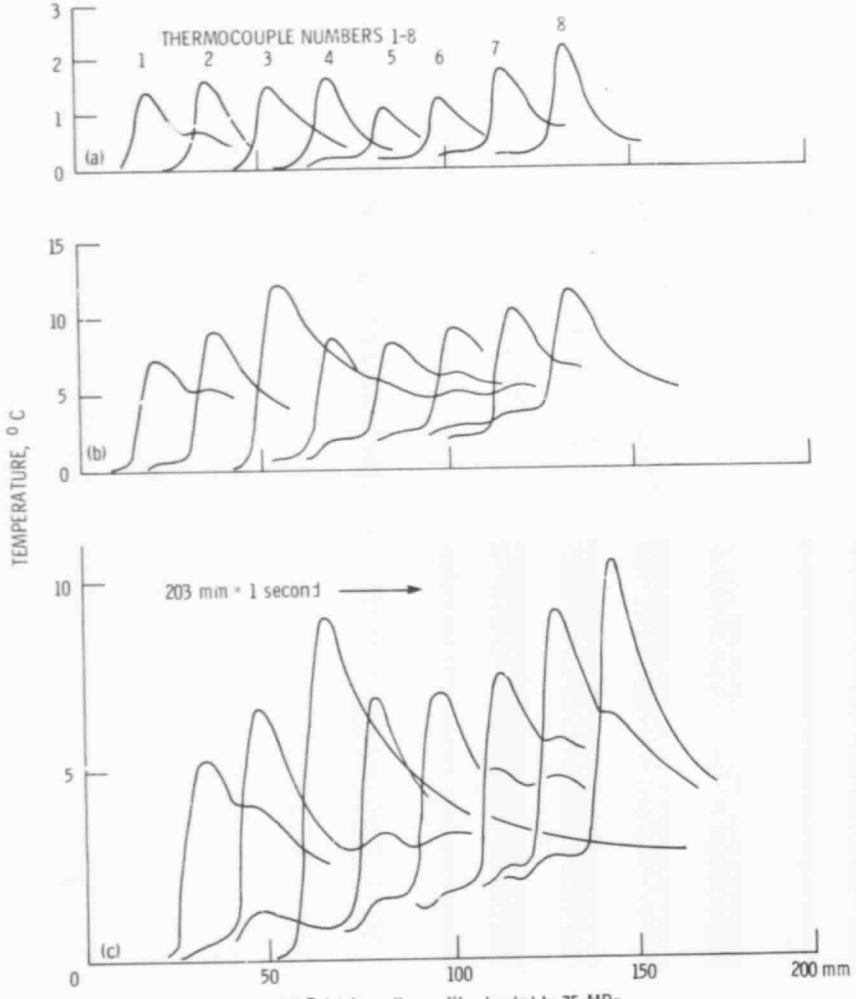

(a) Trichloroethane film loaded to 75 MPa.

(b) Trichloroethane film loaded to 750 MPa.

(c) Solvent film loaded to 520 MPa.

Figure 4. - Comparison of temperature time characteristics of loaded films for a surface velocity of 41.9 mm/s.

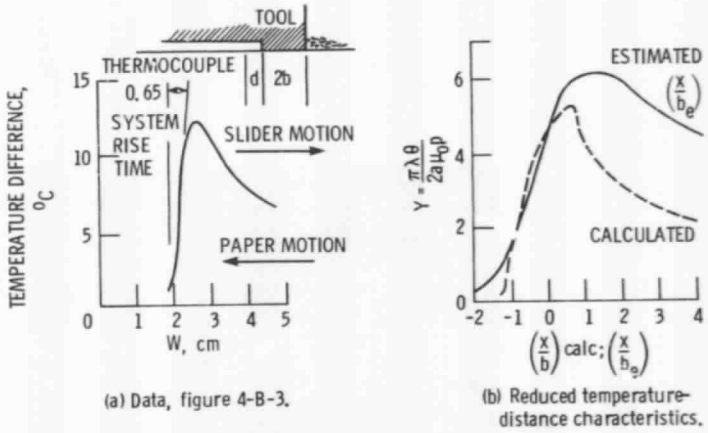

(a) Data, figure 4-B-3.

(b) Reduced temperature-distance characteristics.

Figure 5. - Comparison of theoretical and estimated experimental reduced temperature-distance characteristics for trichloroethane loaded to 750 MPa with a surface velocity of 41.0 mm/s and system response time equivalent to W = 0.65 cm.

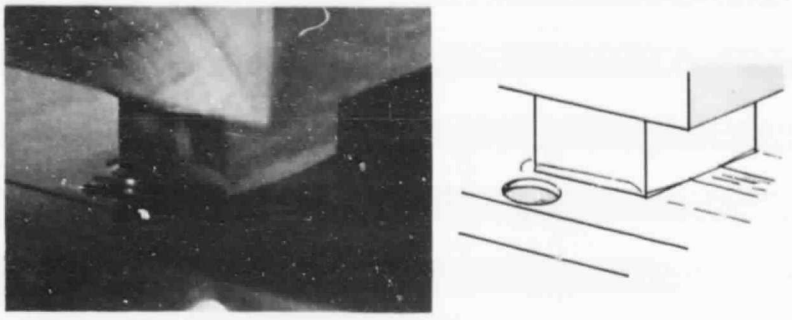

(a) Appearance of a dry streak, Trichloroethane at 450 MPa.

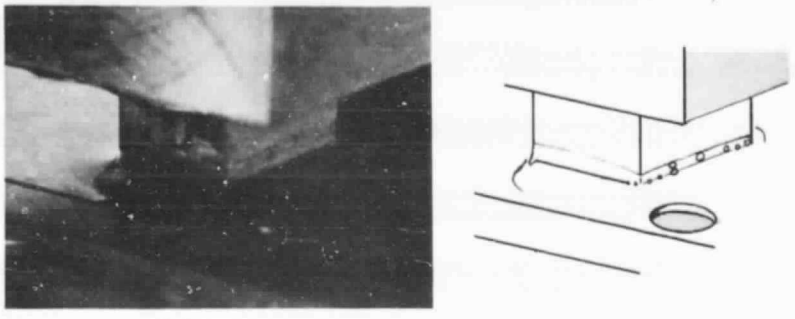

(b) Nucleate boiling off tool trailing edge, Trichloroethane at 600 MPa.

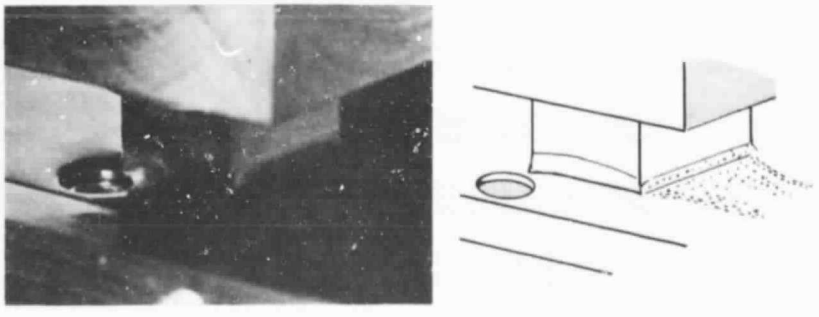

(c) Boiling of volatile component off tool trailing edge, solvent at 450 MPa.

Figure 6. - Selected photographs of slider film behavior under conditions of drying, nucleate boiling and release of volatile component.